

## Correlation between Imaging Markers Derived from PET/MRI and Invasive Acquired Biomarkers in Newly Diagnosed Breast Cancer

Kai Jannusch, Ann-Kathrin Bittner, Nils-Martin Bruckmann, Janna Morawitz, Cleo Stieglitz, Frederic Dietzel, Harald H. Quick, Hideo A. Baba, Ken Herrmann, Lale Umutlu, Gerald Antoch, Julian Kirchner, Sabine Kasimir-Bauer, Oliver Hoffmann

Article - Version of Record



### Suggested Citation:

Jannusch, K., Bittner, A.-K., Bruckmann, N.-M., Morawitz, J., Stieglitz, C., Dietzel, F., Quick, H. H., Baba, H. A., Herrmann, K., Umutlu, L., Antoch, G., Kirchner, J. P., Kasimir-Bauer, S., & Hoffmann, O. (2023). Correlation between Imaging Markers Derived from PET/MRI and Invasive Acquired Biomarkers in Newly Diagnosed Breast Cancer. *Cancers*, 15(6), Article 1651. <https://doi.org/10.3390/cancers15061651>

Wissen, wo das Wissen ist.

This version is available at:

URN: <https://nbn-resolving.org/urn:nbn:de:hbz:061-20250218-113900-6>




Terms of Use:

This work is licensed under the Creative Commons Attribution 4.0 International License.

For more information see: <https://creativecommons.org/licenses/by/4.0>

## Article

# Correlation between Imaging Markers Derived from PET/MRI and Invasive Acquired Biomarkers in Newly Diagnosed Breast Cancer

Kai Jannusch <sup>1</sup>, Ann-Kathrin Bittner <sup>2</sup>, Nils Martin Bruckmann <sup>1</sup>, Janna Morawitz <sup>1</sup>, Cleo Stieglitz <sup>1</sup>, Frederic Dietzel <sup>1</sup> , Harald H. Quick <sup>3,4</sup>, Hideo A. Baba <sup>5</sup>, Ken Herrmann <sup>6</sup>, Lale Umutlu <sup>7</sup>, Gerald Antoch <sup>1</sup>, Julian Kirchner <sup>1,\*</sup> , Sabine Kasimir-Bauer <sup>2</sup>  and Oliver Hoffmann <sup>2</sup>

<sup>1</sup> Department of Diagnostic and Interventional Radiology, University Dusseldorf, Medical Faculty, 40225 Dusseldorf, Germany

<sup>2</sup> Department Gynecology and Obstetrics, University Hospital Essen, University of Duisburg-Essen, 45147 Essen, Germany

<sup>3</sup> High-Field and Hybrid MR Imaging, University Hospital Essen, University Duisburg-Essen, 45147 Essen, Germany

<sup>4</sup> Erwin L. Hahn Institute for Magnetic Resonance Imaging, University Duisburg-Essen, 45141 Essen, Germany

<sup>5</sup> Institute of Pathology, University Hospital Essen, University of Duisburg-Essen, 45147 Essen, Germany

<sup>6</sup> Department of Nuclear Medicine, University Hospital Essen, University of Duisburg-Essen, 45147 Essen, Germany

<sup>7</sup> Department of Diagnostic and Interventional Radiology and Neuroradiology, University Hospital Essen, University of Duisburg-Essen, 45147 Essen, Germany

\* Correspondence: julian.kirchner@med.uni-duesseldorf.de; Tel.: +49-211-8-11-77-54

**Simple Summary:** Histological and molecular breast cancer (BC) characteristics are highly important for individualized therapeutical strategies and personalized risk assessment. Despite the improvement of existing image-based staging examinations over the last years, especially the implementation of PET/MRI examinations at leading tumor centers, the invasive part of BC staging is unavoidable. However, the diagnostic potential of PET/MRI has not yet been fully explored. Thus, this study aimed to analyze possible correlations between PET/MRI imaging markers and invasive acquired biomarkers in newly diagnosed early BC to possibly spare invasive procedures for BC patients in the future. At a population of 169 women a correlation between glucose metabolism and estrogen-receptor and progesterone-receptor expression, Ki67, and tumor grading was shown, whereas no correlation regarding disseminated tumor cells (DTCs) could be found. Thus, [<sup>18</sup>F]FDG-PET/MRI may give a first impression of BC-receptor status and BC-tumor biology during initial staging by measuring glucose metabolism but cannot distinguish between DTC-positive/-negative patients and replace biopsy.

**Abstract:** Purpose: Evaluate the diagnostic potential of [<sup>18</sup>F]FDG-PET/MRI data compared with invasive acquired biomarkers in newly diagnosed early breast cancer (BC). Methods: Altogether 169 women with newly diagnosed BC were included. All underwent a breast- and whole-body [<sup>18</sup>F]FDG-PET/MRI for initial staging. A tumor-adapted volume of interest was placed in the primaries and defined bone regions on each standard uptake value (SUV)/apparent diffusion coefficient (ADC) dataset. Immunohistochemical markers, molecular subtype, tumor grading, and disseminated tumor cells (DTCs) of each patient were assessed after ultrasound-guided biopsy of the primaries and bone marrow (BM) aspiration. Correlation analysis and group comparisons were assessed. Results: A significant inverse correlation of estrogen-receptor (ER) expression and progesterone-receptor (PR) expression towards SUV<sub>max</sub> was found (ER:  $r = 0.27$ ,  $p < 0.01$ ; PR:  $r = 0.19$ ,  $p < 0.05$ ). HER2-receptor expression showed no significant correlation towards SUV and ADC values. A significant positive correlation between Ki67 and SUV<sub>max</sub> and SUV<sub>mean</sub> ( $r = 0.42$ ,  $p < 0.01$ ;  $r = 0.19$ ,  $p < 0.05$ ) was shown. Tumor grading significantly correlated with SUV<sub>max</sub> and SUV<sub>mean</sub> ( $\rho = 0.36$  and  $\rho = 0.39$ , both  $p$ 's  $< 0.01$ ). There were no group differences between SUV/ADC values of DTC-positive/-negative patients. Conclusions: [<sup>18</sup>F]FDG-PET/MRI may give a first impression of BC-receptor status and



**Citation:** Jannusch, K.; Bittner, A.-K.; Bruckmann, N.M.; Morawitz, J.; Stieglitz, C.; Dietzel, F.; Quick, H.H.; Baba, H.A.; Herrmann, K.; Umutlu, L.; et al. Correlation between Imaging Markers Derived from PET/MRI and Invasive Acquired Biomarkers in Newly Diagnosed Breast Cancer. *Cancers* **2023**, *15*, 1651. <https://doi.org/10.3390/cancers15061651>

Academic Editor: Angela Spanu

Received: 13 February 2023

Accepted: 6 March 2023

Published: 8 March 2023



**Copyright:** © 2023 by the authors. Licensee MDPI, Basel, Switzerland. This article is an open access article distributed under the terms and conditions of the Creative Commons Attribution (CC BY) license (<https://creativecommons.org/licenses/by/4.0/>).

BC-tumor biology during initial staging by measuring glucose metabolism but cannot distinguish between DTC-positive/-negative patients and replace biopsy.

**Keywords:** PET/MRI; breast cancer; imaging biopsy; DTC

## 1. Introduction

Worldwide breast cancer (BC) is the most common cancer in women with almost 2.3 million new diagnoses in 2020 [1,2]. Although the 5-year overall survival (OS) rate is about 90% [3] due to improvement in diagnostics and therapy, a considerable number of patients (approximately 20%) with early BC will develop recurrence, depending on the tumor subtype, etc. [4,5]. For personalized clinical risk assessment and developing a therapeutical strategy, accurate pretherapeutic staging is of particular importance after initial diagnosis in early BC. Implementing positron emission tomography/computed tomography (PET/CT) in BC staging improves diagnostics from stage IIb and higher with a focus on distant lymph node metastases providing a higher accuracy compared to single CT staging [6,7]. Furthermore, the PET component improves the accuracy and seems to have an additive predictive potential for disease recurrence in BC and non-BC studies [8–10]. Additionally, PET/magnetic resonance imaging (MRI) is an increasingly important element for BC patients of initial whole-body diagnostics in leading tumor centers and outperforms the staging algorithm currently recommended in BC guidelines as well as PET/CT with a focus on local BC classification and identification of distant metastases [11–18]. This is mainly due to the excellent soft tissue contrast in combination with the obtained multiparametric dataset that allows further tumor classification as well as individual therapeutical strategies [19–21]. Furthermore, PET/MRI has the ability to provide functional data related to tumor biology (e.g., cell replication) by using diffusion-weighted imaging and tumor neoangiogenesis by examining dynamic contrast-enhanced MRI sequences [22]. Invasive diagnostics to determine histopathological and molecular characteristics (e.g., molecular subtypes) of BC tumor cells have become highly important for individualized BC therapies and are unavoidable by now [23–25]. This applies to diagnostics of early micrometastatic tumor spread to the blood and bone marrow (BM), called minimal residual disease (MRD) [26,27], surviving in a state of dormancy, preferentially in the BM as disseminated tumor cells (DTCs) [28]. DTCs are independent prognostic markers for BC OS, disease-free survival (DFS), and distant disease-free survival (DDFS) in multivariate analysis, undetectable by standard staging methods [29].

The diagnostic potential of PET/MRI on a molecular level has not yet been fully explored. Some studies could already highlight the potential of glucose metabolism of different tumor entities (e.g., gliomas, endometrial cancer, lung cancer, BC) measured by SUV at PET data for the determination of tumor aggressiveness, tumor grading, and tumor subtypes [30–34]. Especially significant correlations of BC glucose metabolism towards histological characteristics of BC regarding estrogen (ER, inverse correlation) and progesterone receptor state (PR, inverse correlation) and tumor aggressiveness (Ki67, verse correlation) could be visualized [35,36]. Furthermore, diffusion-weighted imaging (DWI) of MRI data sets achieved during MRI and PET/MRI delivers information about tumor cellularity and helps to distinguish between cancerous and non-cancerous lesions in BC and non-BC studies [37–40]. Additionally, Catalano et al. (2017) found a significant inverse correlation between  $ADC_{mean}$  measurements from PET/MRI towards human epidermal growth factor receptor 2 (HER2) positivity in invasive ductal BC [35]. To the best of our knowledge, there are currently no studies in the actual literature that evaluate the detection of DTCs using image morphological parameters derived from PET/MRI or other radiological imaging modalities.

Summing up, the individual characterization of BC tumor cells and treatment of BC is substantially and currently an interplay of invasive and imaging diagnostics. In order to

deepen the understanding of BC tissue on a molecular level and to supplement the required invasive diagnostics in the future, this study should analyze possible correlations between imaging markers derived from PET/MRI and invasive acquired markers/tumor biology in newly diagnosed early BC on a clinically feasible basis.

## 2. Materials and Methods

### 2.1. Patients

The institutional review boards of the University Duisburg-Essen, Germany (study number 17-7396-BO) and Düsseldorf, Germany (study number 6040R) approved this study and it was performed in conformance with the Declaration of Helsinki [41]. Data acquisition was performed between March 2018 and December 2021. Women with newly diagnosed, therapy-naïve early BC were included in this retrospective trial and all patients met the following inclusion criteria: (i) tumors presenting with at least cT2 tumor stage; (ii) triple-negative BC (TNBC) of any tumor size; or (iii) tumors with intermediate risk due to clinicopathological parameters, without having performed multigene assays at that point or high risk, presenting with at least one of the following characteristics:  $>cT1c$ ,  $Ki67 > 14\%$ , HER2 overexpression, G3. The following exclusivity criteria have been defined: (i) former malignancies within the last five years, (ii) contraindications to MRI or MRI contrast agents, and (iii) pregnancy or breastfeeding. Written informed consent form was obtained from all patients. All patients underwent a dedicated breast [ $^{18}F$ ]FDG-PET/MRI for initial staging purposes.

### 2.2. PET/MRI

The dedicated [ $^{18}F$ ]FDG-PET/MRI examinations were performed on an integrated 3-Tesla PET/MRI system (Biograph mMR, Siemens Healthcare GmbH, Erlangen, Germany). The average delay was  $69 \pm 15$  min after injection of bodyweight-adapted dosage of [ $^{18}F$ ]FDG (4 MBq/kg bodyweight). To ensure blood glucose levels of below 150 mg/dL, blood samples were obtained and patients need to fast six hours prior to injection.

The first examination was a dedicated and comprehensive breast-[ $^{18}F$ ]FDG-PET/MRI examination, performed in a head-first prone position utilizing a dedicated 16-channel radiofrequency (RF) breast coil (Rapid Biomedical, Rimpf, Germany), developed and designed for use in integrated whole-body PET/MR imaging [42]. PET data and MRI data of both breasts were acquired simultaneously with an acquisition time of 20 min per bed position. PET image reconstruction was performed subsequently using an iterative ordered subset expectation maximization algorithm, 3 iterations and 21 subsets, a Gaussian filter with 4 mm full width at half maximum, and a  $256 \times 256$  image matrix. PET data of the patient tissues were automatically attenuation corrected using an implemented four-compartment model attenuation map ( $\mu$ -map) calculated from fat-only and water-only data sets, as obtained by Dixon-based sequences. The attenuation correction for the 16-channel RF breast coil was automatically performed by the PET/MRI system. A 3D attenuation template of the RF breast coil based on CT data was implemented into the PET data reconstruction process for this purpose [42].

The dedicated breast MRI protocol comprised the following sequences:

- (i) A transversal T2-weighted (T2w) turbo-spin echo (TSE) fat-saturated sequence with a slice thickness of 7 mm (TE 97 ms; TR 2840 ms; FOV 400 mm; phase FOV 75%; acquisition matrix  $256 \times 192$ , in-plane resolution  $1.6 \times 1.6$  mm<sup>2</sup>)
- (ii) A transversal diffusion-weighted echo-planar imaging (EPI) sequence with a slice thickness of 5.0 mm (TR 8000 ms; TE 81 ms; b-values: 0, 400 and 800 s/mm<sup>2</sup>, matrix size  $192 \times 156$ ; FOV 420 mm, phase FOV, 81.3%; GRAPPA, acceleration factor 2; in-plane resolution  $2.2 \times 2.2$  mm<sup>2</sup>)
- (iii) Six repetitions of a transversal 3-dimensional fast low-angle shot (FLASH) T1w sequence with a slice thickness of 7 mm (TE 3.62 ms; TR 185 ms; FOV 400 mm; phase FOV 75%; acquisition matrix  $320 \times 240$ , in-plane resolution  $1.3 \times 1.3$  mm<sup>2</sup>) for dynamic contrast-enhanced imaging. A dose of 0.2 mmol/kg bodyweight gadoterate

meglumine (Dotarem, Guerbet, Sulzbach, Germany) was injected intravenously after the first FLASH sequence with a flow of 2 mL/s using an automated injector (Spectris Solaris, MR Injection System; Medrad, Pittsburgh, PA, USA). Subsequent automated image subtraction was performed.

Subsequent to the dedicated breast [ $^{18}\text{F}$ ]FDG-PET/MRI examination patients were positioned head-first-supine for a second whole-body [ $^{18}\text{F}$ ]FDG-PET/MRI examination. Data acquisition was performed in 4–5 bed positions with an acquisition time of three min per bed position. The following vendor-provided RF coils for MR signal reception that are part of the PET/MR system were used: (i) 16-channel head/neck RF coil (ii) 24-channel spine-array RF coil (iii) 3–4 flexible body array RF coils each with six channels for whole-body coverage (head to mid-thigh). Both the head/neck and spine-array RF coil are included in the automated attenuation correction procedure of the PET/MRI system [43]. The flexible-body array RF coils are designed as PET-transparent as possible and are not considered in the attenuation correction procedure [44,45].

All PET images were reconstructed using the iterative ordered-subset expectation maximization (OSEM) algorithm, three iterations, 21 subsets, a Gaussian filter with 4 mm full width at half maximum (FWHM), and a  $344 \times 344$  image matrix. For MR-based attenuation correction of the patient tissues, a two-point (fat, water) coronal 3D-Dixon-VIBE sequence was acquired to generate a four-compartment model (background air, lungs, fat, muscle).

The dedicated whole-body [ $^{18}\text{F}$ ]FDG-PET/MRI examination comprised the following sequences:

- (i) A transverse T2-w half Fourier acquisition single-shot turbo spin echo (HASTE) sequence in breath-hold technique with a slice thickness of 7 mm (TE 97 ms; TR 1500 ms; turbo factor (TF) 194; FOV 400 mm; phase FOV 75%; acquisition matrix  $320 \times 240$  mm; in-plane resolution  $1.3 \times 1.3$  mm<sup>2</sup>; TA 0:47 min/bed position)
- (ii) A transversal diffusion-weighted (DWI) echo-planar imaging (EPI) sequence in free breathing with a slice thickness of 5.0 mm (TR 7400 ms; TE 72 ms; b-values: 0, 500 and 1000 s/mm<sup>2</sup>, matrix size  $160 \times 90$ ; FOV 400, phase FOV, 75%; GRAPPA, acceleration factor 2; in-plane resolution  $2.6 \times 2.6$  mm<sup>2</sup>; TA 2:06 min/bed position)
- (iii) A fat-saturated post-contrast transverse 3-dimensional volumetric interpolated breath-hold examination (VIBE) sequence with a slice thickness of 3 mm (TE, 1.53 ms; TR, 3.64 ms; flip angle 9°; FOV 400; phase FOV 75%; acquisition matrix  $512 \times 384$ , in-plane resolution  $0.7 \times 0.7$  mm<sup>2</sup>; TA 0:19 min/bed position)

### 2.3. Image Analysis

All images were analyzed using a dedicated OsiriX workstation (Version 9.0.2; Pixmeo SARL, Bernex, Switzerland). A breast-imaging specialist with more than 10 years of experience and a hybrid-imaging specialist with two years of experience performed the data evaluation.

**Breast lesion:** After defining the malign breast lesion at T1 weighted post-contrast sequence, a tumor size adapted volume of interest (VOI) that adequately captured the breast cancer lesion was set in the ADC map of each patient. Afterward, the VOI was copied to the corresponding PET images to match the identical plane and position. Finally, in both images, a manual reshape was performed to avoid pixel loss (Figure 1).

**Bone marrow:** Matching with transverse T1-weighted post-contrast sequence, a bone size adapted VOI (on average 1.0 cm spherical diameter) was placed in the ADC map centrally in each of the following bones: femur right, os sacrum, os ilium right, lumbar vertebral body 5 (L 5), thoracic vertebral body 7 (T 7), and sternum. Afterward, the VOI was copied to the corresponding PET images to match the identical plane and position. Finally, in both images, a manual reshape was performed to avoid pixel loss (Figure 2).



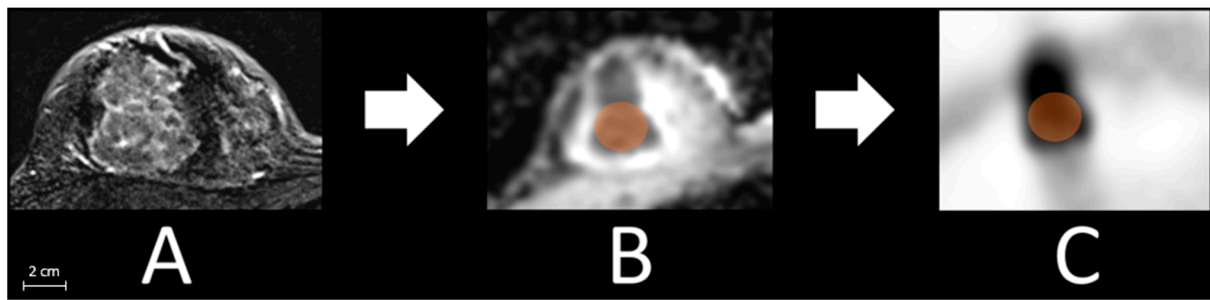


**Figure 1.** Exemplified measurement processes with detecting the lesion in T1 weighted post-contrast sequence (A), placing a tumor size adapted volume of interest (VOI, orange, 2.3 cm here) in the ADC map (B), and afterward copying the VOI to the corresponding slice of the PET images (C).

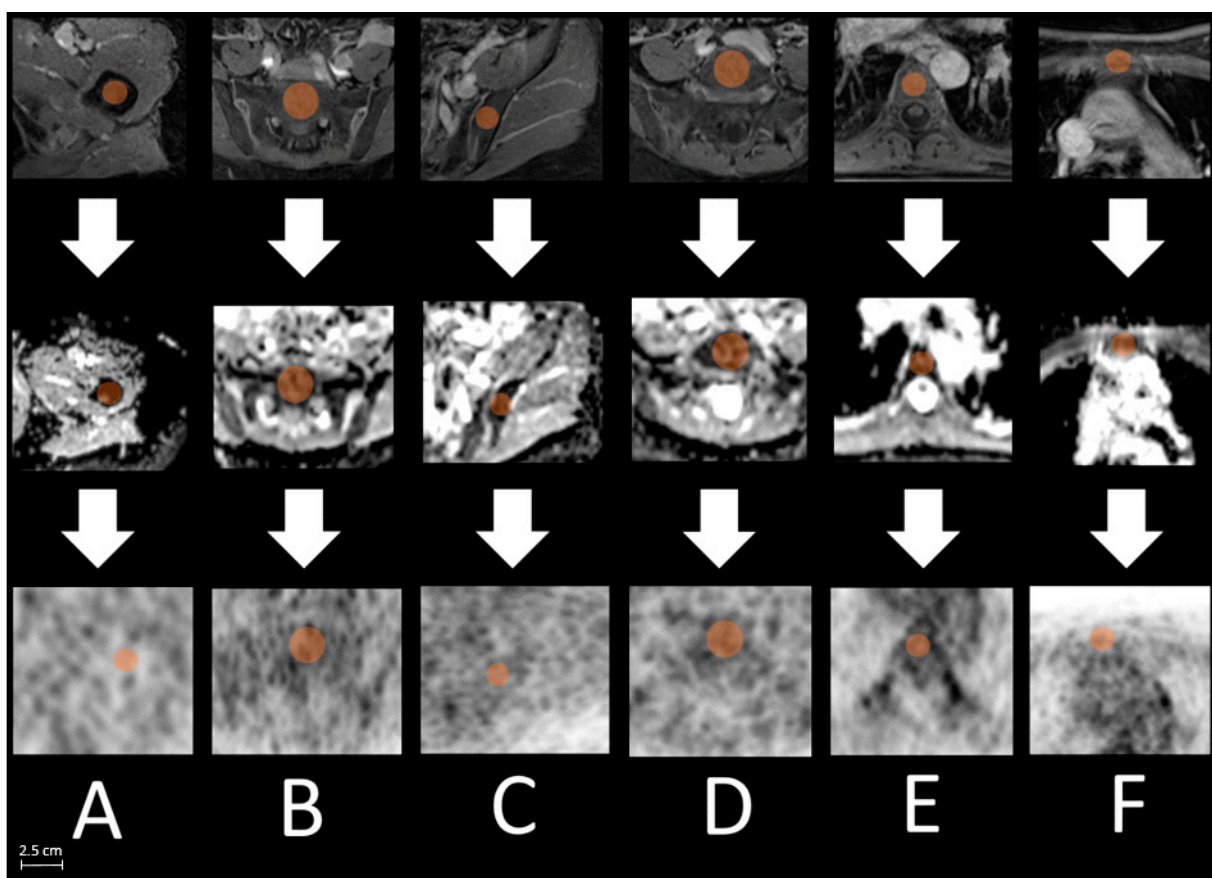


**Figure 2.** Exemplified measurement processes with locating defined bone regions ((A): right femur, (B): os sacrum, (C): os ilium, (D): L 5, (E): T 7, (F): sternum) in T1 weighted post-contrast sequence ((upper) row), placing a bone size adapted volume of interest (VOI, orange, max. 2.5 cm os sacrum) centrally in each bone location in the ADC map ((middle) row) and afterward copying the VOI to the corresponding slice of the PET images ((lower) row).

OsiriX automatically calculated  $SUV_{max}$  and  $SUV_{mean}$  from PET, and  $ADC_{mean}$  from DWI of each PET/MRI data set. In partly included pixels, the software used subpixel interpolation.

#### 2.4. Histopathological Examination

For each patient, tumor grading (G1–G3), type, and tumor biology including estrogen (ER) and progesterone receptor (PR), as well as human epidermal growth factor receptor 2 (HER2) status and Ki67 (proliferation marker) were assessed according to World Health Organization classification after ultrasound-guided biopsy. Tumor biology as well as tumor

subtypes are essential for therapeutic strategies [46]. Patients were divided into subgroups: Luminal-A-like, Luminal-B-like HER2 negative, TNBC, and HER2 positive [47,48].

### 2.5. Selection and Detection of Disseminated Tumor Cells (DTCs)

Between 10 and 20 mL BM was aspirated from the anterior iliac crests of all patients at the beginning of surgery of the primary tumor, before the start of any therapy, and processed within 24 h. DTC isolation and detection were performed on the basis of the recommendations for standardized tumor cell detection, published by the German consensus group of Senology [49]. Details of the staining procedure, for example, the number of evaluated slides, controls, and cell detection, have been described elsewhere [50]. Briefly, BM cells were isolated from heparinized BM (5000 U/mL bone marrow) by Ficoll–Hypaque density gradient centrifugation (density 1.077 g/mol; Pharmacia) at  $400 \times g$  for 30 min. Slides were analyzed for DTCs by immunocytochemistry using the pan-cytokeratin anti-body A45-B/B3 (see Figure 3). Microscopic evaluation of the slides was carried out using the ARIOL system (Applied Imaging, San José, CA, USA), according to the ISHAGE evaluation criteria [51].

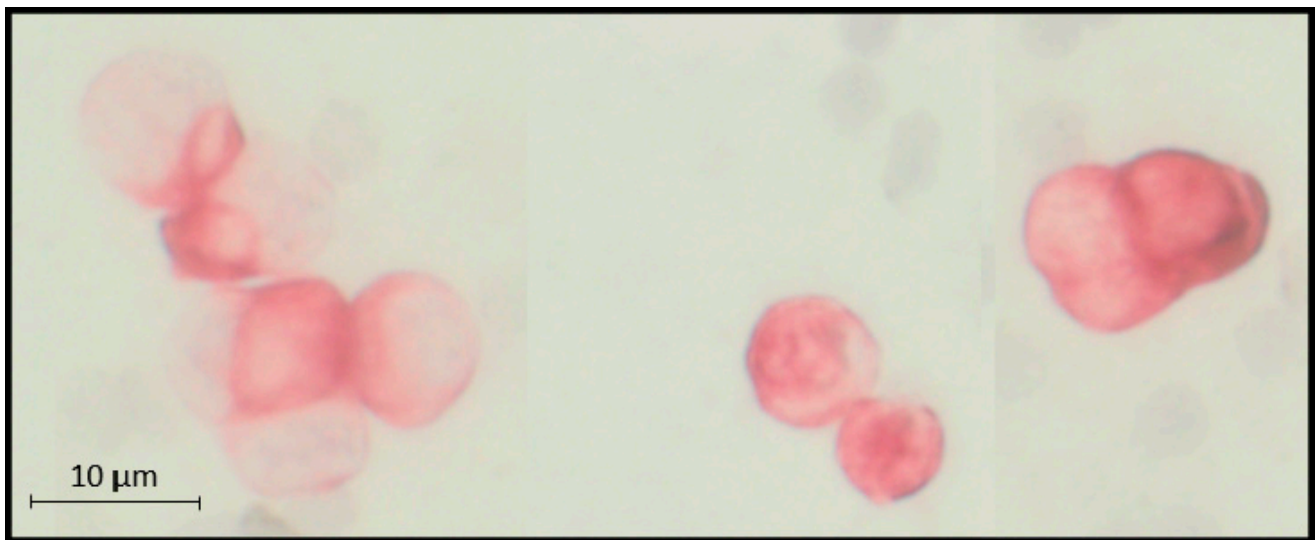


**Figure 3.** Example of microscopic visualized cytokeratin-positive disseminated tumor cells (on average 11  $\mu$ m) in bone marrow aspirate from the anterior iliac crests.

### 2.6. Statistical Analysis

Statistical analysis was performed using SPSS Statistics 26 (IBM Corp, Chicago, IL, USA). Pearson's (ER, PR, Ki67) and Spearman's (HER2/neu, molecular subtype, tumor grading) correlation coefficients were calculated to correlate  $SUV_{max}/SUV_{mean}$  and  $ADC_{mean}$  tumor values and immunohistochemical markers or tumor grading. The Mann–Whitney-U-Test was used for group comparison of  $SUV/ADC$  values of DTC-positive or -negative patients at defined bone regions. A  $p$ -value less than 0.05 was considered statistically significant. Data are presented as mean  $\pm$  standard deviation.

## 3. Results

### 3.1. Patient Population and Histopathological Findings

A total of 169 female patients ( $56 \pm 12$  years) were included in this retrospective trial. For the distribution of the cohort into molecular subtypes and tumor grading, see Table 1.

### 3.2. Correlation of Breast Cancer SUV and ADC with Histopathological Breast Cancer Parameters

ER expression was found in 124/169 (73%) patients with a mean expression of  $83 \pm 29\%$  and a significant inverse correlation with  $SUV_{max}$  ( $r = 0.27$  and  $p < 0.01$ ). No significant correlation between ER and  $SUV_{mean}/ADC$  could be found. PR expression was

detected in 115/169 (68%) patients with a mean expression of  $58 \pm 37\%$  and a significant inverse  $SUV_{max}$  correlation ( $r = 0.19$  and  $p < 0.05$ ). No significant correlation between PR and  $SUV_{mean}/ADC$  was found. HER2 receptor expression was described in 97/169 (57%) patients, showing no significant correlations with SUV and ADC values. The mean Ki67 was  $43 \pm 27\%$  and showed a significant positive correlation with  $SUV_{max}$  and  $SUV_{mean}$  ( $r = 0.42$   $p < 0.01$ ;  $r = 0.19$ ,  $p < 0.05$ ). No significant correlation between the Ki67 index and ADC was found, as well as between molecular subtypes with SUV/ADC. A significant positive correlation of tumor grading with  $SUV_{max}$  and  $SUV_{mean}$  could be shown ( $\rho = 0.36$  and  $\rho = 0.39$ , both  $p$ 's  $< 0.01$ ), whereas no significant correlation between tumor grading and ADC was found (Table 2 and Figure 4).

**Table 1.** Distribution of the cohort (n = 169) into (A) molecular subtypes and (B) tumor grading.

A	Molecular Subtypes	Luminal A	Luminal B HER2—	Triple Negative	HER2+
	total 169	7 (4%)	42 (25%)	23 (14%)	97 (57%)
B	Tumor Grading	Grade 1	Grade 2	Grade 3	
	total 169	3 (2%)	100 (59%)	66 (39%)	

**Table 2.** Correlation between immunohistochemical markers (estrogen, progesterone, HER2, Ki67), molecular subtype, tumor grading in relation to SUV, and ADC measurements from [ $^{18}F$ ]FDG-PET/MRI.

	Malign Breast Lesion PET/MRI		
	$SUV_{max}$	$SUV_{mean}$	$ADC_{mean}$
Estrogen	$r = -0.27^{**}$	$r = -0.07$	$r = -0.06$
Progesterone	$r = -0.19^{*}$	$r = -0.11$	$r = -0.15$
HER2/neu	$\rho = -0.07$	$\rho = -0.04$	$\rho = -0.06$
Ki67	$r = 0.42^{**}$	$r = 0.19^{*}$	$r = -0.08$
Molecular subtype	$\rho = 0.04$	$\rho = 0.06$	$\rho = -0.01$
Tumor grading	$\rho = 0.36^{**}$	$\rho = 0.39^{**}$	$\rho = 0.02$

\* Bold values indicate significance at  $p < 0.05$ /\*\* Bold values indicate significance at  $p < 0.01$ .

### 3.3. Group Comparison of Bone Marrow SUV/ADC between DTC-Positive and DTC-Negative Patients

In a subgroup of 136 patients, BM was evaluated for DTCs. Due to image artifacts (e.g., after artificial hip implantation), 13 of those patients were excluded from further analysis respective to bone regions (n = 5 right femur, n = 2 os sacrum, n = 2 right os ilium, n = 1 L 5, n = 3 sternum).

The Mann–Whitney-U-Test revealed no significant differences of SUV/ADC values derived from [ $^{18}F$ ]FDG-PET/MRI between DTC-positive and DTC-negative patients concerning defined BM regions: right femur, os sacrum, right os ilium, L 5, T 7, and sternum. For detailed data visualization, see Table 3 and Figures 5 and 6.



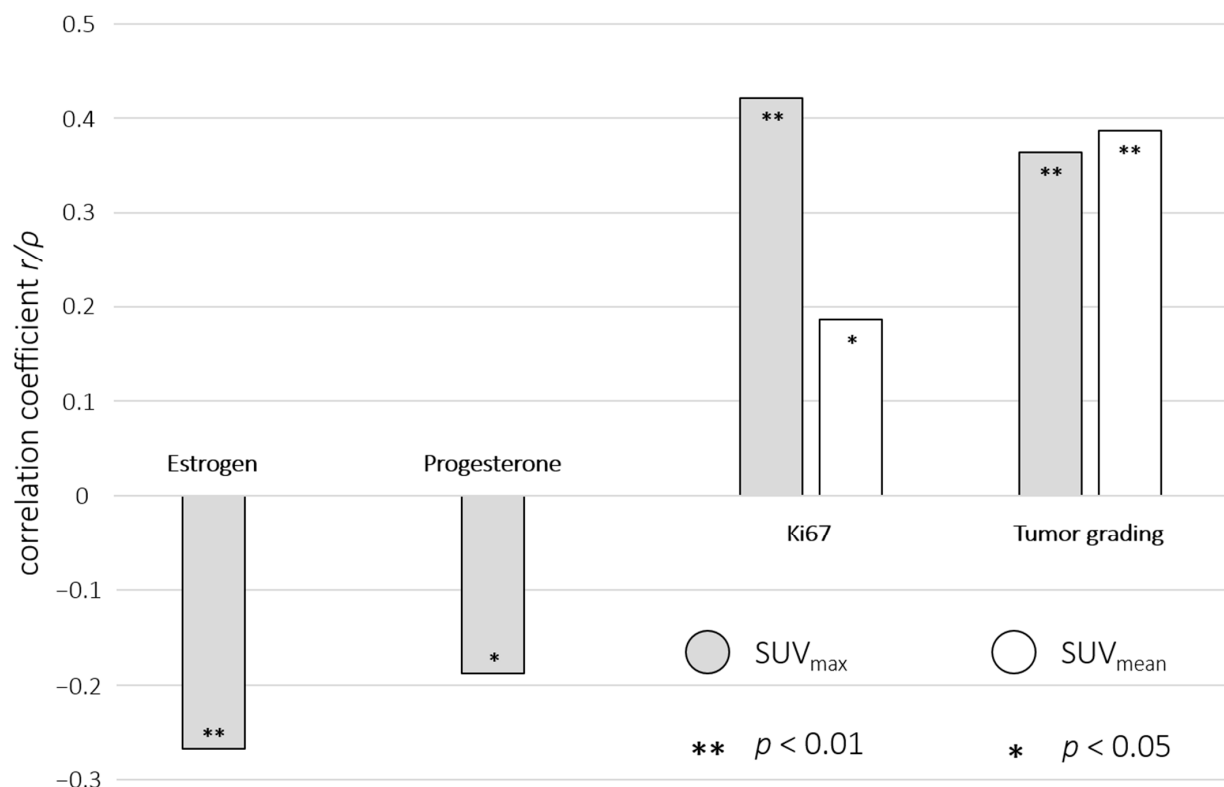


**Figure 4.** Visualized significant correlations between immunohistochemical markers, tumor grading, and SUV<sub>max</sub> (grey)/SUV<sub>mean</sub> (white) from [<sup>18</sup>F]FDG-PET/MRI in combination with their correlation coefficients ( $r/\rho$ ) and  $p$  values (\*\*  $p < 0.01$ ; \*  $p < 0.05$ ).

**Table 3.** Comparison of SUV<sub>max</sub>/SUV<sub>mean</sub>/ADC<sub>mean</sub> values derived from defined BM regions at [<sup>18</sup>F]FDG-PET/MRI between DTC-positive and DTC-negative patients using Mann–Whitney-U test. Descriptive group statistics (median (*Mdn*), interquartile range (*IQR*)) and results of Mann–Whitney-U test are visualized.

		SUV <sub>max</sub>		SUV <sub>mean</sub>		ADC <sub>mean</sub>	
		DTC-Negative	DTC-Positive	DTC-Negative	DTC-Positive	DTC-Negative	DTC-Positive
Right femur	<i>Mdn</i> ( <i>IQR</i> )	2.01 (1.27)	2.06 (1.18)	0.81 (0.46)	0.80 (0.45)	406.33 (334.25)	389.45 (284.17)
	Mann–Whitney-U	$U = 1880.00, Z = -0.61, p = 0.54, r_{rb} = -0.05$		$U = 1940.50, Z = -0.33, p = 0.75, r_{rb} = -0.03$		$U = 1950.00, Z = -0.28, p = 0.78, r_{rb} = -0.03$	
Os sacrum	<i>Mdn</i> ( <i>IQR</i> )	3.26 (1.23)	3.31 (1.34)	1.54 (0.46)	1.53 (0.51)	508.94 (196.60)	438.55 (233.28)
	Mann–Whitney-U	$U = 2099.00, Z = -0.31, p = 0.76, r_{rb} = 0.03$		$U = 2149.00, Z = -0.08, p = 0.93, r_{rb} = -0.01$		$U = 1724.00, Z = -1.73, p = 0.08, r_{rb} = -0.15$	
Right os ilium	<i>Mdn</i> ( <i>IQR</i> )	2.85 (1.39)	2.06 (1.18)	1.52 (0.66)	1.44 (0.52)	610.32 (206.80)	622.52 (216.27)
	Mann–Whitney-U	$U = 1626.00, Z = -0.17, p = 0.86, r_{rb} = 0.02$		$U = 2138.50, Z = -0.13, p = 0.90, r_{rb} = -0.01$		$U = 2011.00, Z = -0.41, p = 0.68, r_{rb} = -0.04$	
L5	<i>Mdn</i> ( <i>IQR</i> )	3.05 (1.35)	3.21 (1.22)	1.61 (0.67)	1.61 (0.64)	528.70 (268.14)	547.02 (218.11)
	Mann–Whitney-U	$U = 2005.50, Z = -0.62, p = 0.54, r_{rb} = 0.05$		$U = 1949.00, Z = -0.88, p = 0.38, r_{rb} = -0.08$		$U = 2071.00, Z = -0.13, p = 0.89, r_{rb} = -0.01$	
T7	<i>Mdn</i> ( <i>IQR</i> )	3.61 (1.52)	3.92 (1.11)	2.00 (0.72)	2.03 (0.56)	461.64 (200.83)	411.32 (258.80)
	Mann–Whitney-U	$U = 2018.00, Z = -0.67, p = 0.50, r_{rb} = 0.06$		$U = 2141.00, Z = -0.12, p = 0.91, r_{rb} = -0.01$		$U = 1866.00, Z = -1.36, p = 0.18, r_{rb} = -0.12$	
Sternum	<i>Mdn</i> ( <i>IQR</i> )	1.76 (0.74)	1.75 (0.96)	0.89 (0.41)	0.88 (0.37)	616.46 (232.97)	597.26 (244.70)
	Mann–Whitney-U	$U = 1990.00, Z = -0.80, p = 0.43, r_{rb} = 0.07$		$U = 2122.00, Z = -0.21, p = 0.84, r_{rb} = 0.02$		$U = 1950.00, Z = -0.58, p = 0.56, r_{rb} = -0.05$	

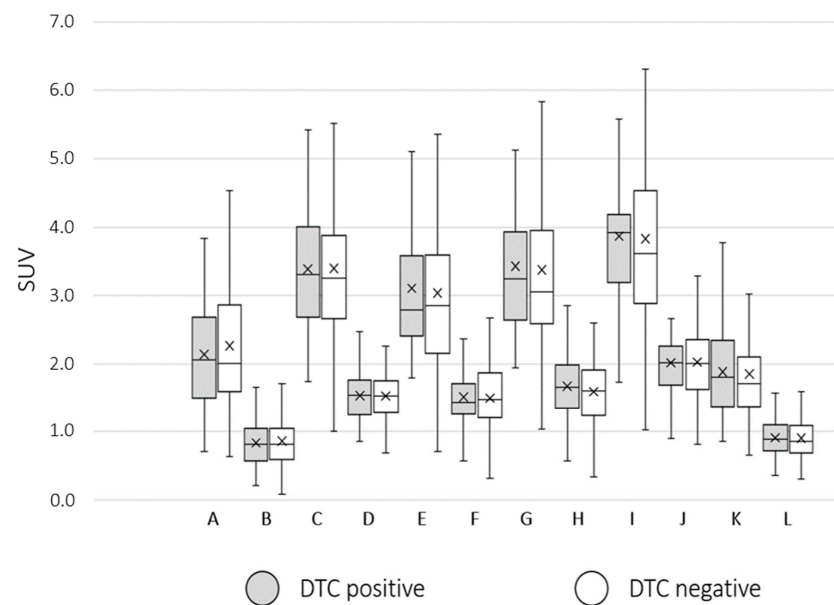


**Figure 5.** Group comparison between DTC (disseminated tumor cells)-positive (grey box) and DTC-negative (white box) patients towards measured SUV bone marrow values: (A) femur right-SUV<sub>max</sub>, (B) right femur SUV<sub>mean</sub>, (C) os sacrum-SUV<sub>max</sub>, (D) os sacrum-SUV<sub>mean</sub>, (E) right os ilium SUV<sub>max</sub>, (F) right os ilium SUV<sub>mean</sub>, (G) L 5-SUV<sub>max</sub>, (H) L 5-SUV<sub>mean</sub>, (I) T 7-SUV<sub>max</sub>, (J) T 7-SUV<sub>mean</sub>, (K) sternum-SUV<sub>max</sub>, and (L) sternum-SUV<sub>mean</sub>. The crosses indicate the mean values. No significant differences in group comparison were visible.

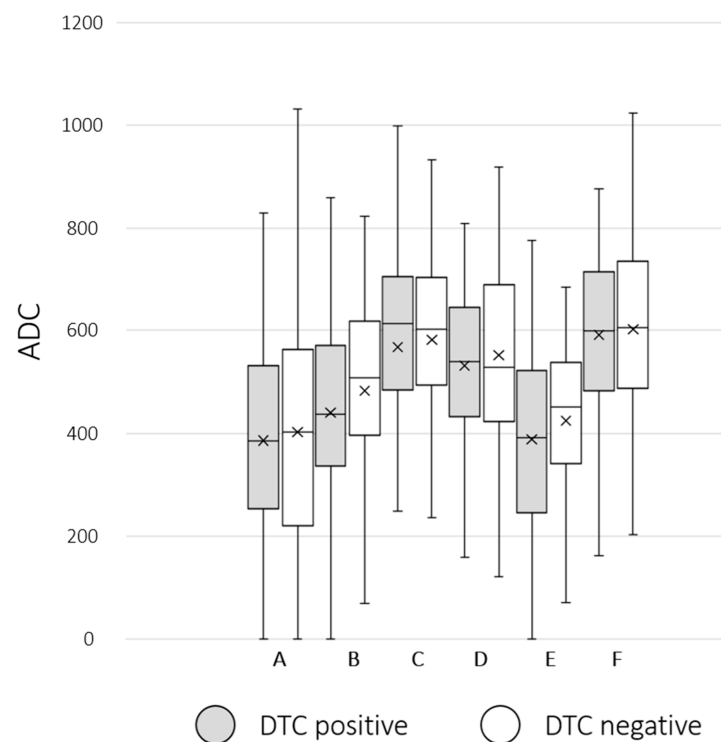


**Figure 6.** Group comparison between DTC (disseminated tumor cells)-positive (grey box) and DTC-negative (white box) patients regarding ADC<sub>mean</sub> bone marrow values: (A) right femur ADC<sub>mean</sub>, (B) os sacrum-ADC<sub>mean</sub>, (C) right os ilium ADC<sub>mean</sub>, (D) L 5-ADC<sub>mean</sub>, (E) T 7-ADC<sub>mean</sub>, and (F) sternum-ADC<sub>mean</sub>. The crosses indicate the mean value. No significant differences in group comparison were visible.

#### 4. Discussion

Histological as well as molecular BC characteristics are highly important for individualized therapeutical strategies and personalized risk assessment [23]. Despite the improvement of existing image-based staging examinations over the last years, especially the implementation of PET/MRI examinations at leading tumor centers, the invasive part of BC staging is unavoidable. Thus, a biopsy of the primary breast lesion for immunohistochemical data is state-of-the-art. BM aspiration has been performed in many clinics several years ago; however, nowadays, due to time-consuming and cost-effective issues, only a very few still perform it to evaluate DTCs. Nevertheless, the informative potential of hybrid examinations such as PET/MRI is not yet exhausted.

To better understand the influence of histopathological and molecular BC characteristics on imaging markers derived from [ $^{18}\text{F}$ ]FDG-PET/MRI, this study aimed to analyze the possible correlations between PET/MRI imaging markers and invasive acquired biomarkers in newly diagnosed early BC patients on a clinically feasible basis. Thus, it could improve personalized clinical risk assessment and the development of therapeutical strategies.

Concordant with Catalano et al. (2017), we found an inverse correlation between  $\text{SUV}_{\text{max}}$  of the malign BC lesion and both ER and PR expression [35]. Thus, a higher  $\text{SUV}_{\text{max}}$  might indicate a lower ER and PR expression. This might be helpful for personalized therapy planning as it is known that information about receptor expression is one necessary component. According to our data information about HER2, expression was not reflected by image morphological data of [ $^{18}\text{F}$ ]FDG-PET/MRI. Ki67 and tumor grading positively correlated with  $\text{SUV}_{\text{max}}$  and  $\text{SUV}_{\text{mean}}$  of the malign BC lesion. Similar supporting results were presented by other BC and non-BC studies [36,52–56]. The amount of Ki67 as well as tumor grading indicate the aggressiveness of BC lesions [57,58]. Consequently, the detected positive correlation of both parameters towards SUV values derived from [ $^{18}\text{F}$ ]FDG-PET/MRI could give an impression of the tumor aggressiveness during initial staging by measuring SUV values. In patients with more than one malignant breast lesion, this correlation provides the opportunity, if not already performed at the initial puncture, to specifically puncture the breast lesion suspected to have the highest malignant potential at [ $^{18}\text{F}$ ]FDG-PET/MRI. Furthermore, Afkari et al. (2021) could show a positive correlation between Ki67 and the risk of bone metastases [59]. As a fast and easily achievable imaging parameter during staging, this might help to improve the staging process giving the investigator the hint that a close look to exclude bone metastases is particularly necessary here [59].

Contrary to Koo et al. (2016), based on our data, there were no significant correlations between molecular subtypes and SUV/ADC values [60]. One potential explanation could be the intermediate- to high-risk population of our cohort including only a small number of patients with Luminal A (4% vs. 60%) tumors and a high amount of HER2-positive (53% vs. 11%) cases [60]. Thus, a group differentiation based on SUV/ADC might be difficult here. Furthermore, there were no correlations of immunohistochemical markers, molecular subtype, and tumor grading toward  $\text{ADC}_{\text{mean}}$  values, which supports the result of some other studies in the current literature [34,35,61,62].

DTCs, detected in BM in about 30% of BC patients, are an independent prognostic marker for disease outcome [27,29]. One therapeutic approach showing an improvement in OS is the application of bisphosphonates [63,64]. Besides reducing skeletal complications, clodronate (clodronic acid) has shown a significant reduction of recurrence to the bone as well as visceral metastasis [65–68]. Moreover, in a small pilot study, we demonstrated a positive effect of ibandronate treatment on the eradication of DTCs, still present 2–10 years after primary diagnosis [68] which was shown to successfully improve outcomes in primary as well as locally advanced BC patients receiving adjuvant/neoadjuvant chemotherapy [50,67]. Unfortunately, DTCs are undetectable by standard staging methods and BM aspiration is needed [69]. Changes in [ $^{18}\text{F}$ ]FDG-PET/MRI imaging markers (SUV/ADC) of the BM in case of DTC positivity would help to spare patients a BM biopsy. According to our data, there is no hint that the existence of DTCs changes [ $^{18}\text{F}$ ]FDG-PET/MRI imaging

markers. The results fit well with the underlying pathophysiology of the disease [70]. As described previously, DTCs are the result of a micrometastatic tumor spread; however, we here only can describe the presence of cytokeratin-positive cells without any further characterization of the cells. Although little is known about the survival conditions of DTCs in the BM, some DTCs have been shown to have stem cell characteristics with the ability of self-renewal [71,72], and we recently demonstrated that early-stage-diagnosed BC patients harboring DTCs expressing the chemokine receptor type 4 (CXCR4) and the transcription factor JUNB had a higher risk for relapse [73]. Furthermore, DTCs have to adapt to new environmental conditions. In this regard, a subpopulation of osteoblasts was identified that was manipulated in their function by DTCs, so-called educated osteoblasts, which in turn crosstalk with DTCs via proteins and soluble factors leading to a reduction in BC cell proliferation and metastatic latency [74]. Dormant DTCs would probably not cause any significant metabolic activity in these cells, which is essential for the accumulation of [ $^{18}\text{F}$ ]FDG. However, only a comprehensive characterization of DTCs, not feasible in daily clinical routines, could finally answer that question. Moreover, DTCs are rarely building larger cell clusters. Thus, the missing metabolic activity and the distribution of DTCs make it actually hard to visualize bone marrow SUV and ADC changes at highly accurate [ $^{18}\text{F}$ ]FDG-PET/MRI staging in a clinical implementable setting.

As a one-stop examination, [ $^{18}\text{F}$ ]FDG-PET/MRI has a significant advantage for BC patients [14–16]. Switching between different modalities and scheduling different appointments during guideline-compliant staging is reduced by implementing PET/MRI as a staging method of choice in leading tumor centers. A further major strength of hybrid imaging is the ability to acquire a multiparametric data set. In particular, since the limitations of this examination have not yet been finally clarified, it would be of great advantage for BC patients to identify histopathological characteristics of the tumor within the imaging process (imaging biopsy).

The visualized [ $^{18}\text{F}$ ]PET association with receptor status and histopathological parameters might help predict BC types and identify BC lesions with the highest malignant potential and thus improves personalized therapy planning with guide-targeted therapies. Nonetheless, [ $^{18}\text{F}$ ]FDG-PET/MRI might find one of its limitations in replacing the BM aspiration to evaluate the DTC status of the patients.

This study has some limitations. First, we only evaluated 136/169 patients' data regarding BM. Nevertheless, this is the first study that evaluates if [ $^{18}\text{F}$ ]FDG-PET/MRI can replace a BM aspiration for the detection of DTCs. Furthermore, histopathological sampling was derived from core needle biopsy; therefore, the biopsy did eventually not represent the whole lesion, which is a well-known problem of other BC studies.

## 5. Conclusions

[ $^{18}\text{F}$ ]FDG-PET/MRI may give a first impression of BC-receptor status and tumor biology during initial staging by measuring glucose metabolism but cannot distinguish between DTC-positive/-negative patients. Thus, regarding multicentricity, it could improve personalized therapy planning with guide-targeted therapies but cannot replace biopsy.

**Author Contributions:** Conceptualization, A.-K.B., J.K. and O.H.; Data curation, K.J., N.M.B., J.M., C.S., F.D., H.H.Q., H.A.B. and S.K.-B.; Formal analysis, K.J.; Investigation, K.J., A.-K.B., J.K. and O.H.; Methodology, A.-K.B., J.K. and O.H.; Resources, K.H., L.U. and G.A.; Supervision, A.-K.B., K.H., L.U., G.A., J.K. and O.H.; Validation, K.J.; Visualization, K.J.; Writing—original draft, K.J.; Writing—review and editing, A.-K.B., N.M.B., J.M., C.S., F.D., H.H.Q., H.A.B., K.H., L.U., G.A., J.K., S.K.-B. and O.H. All authors have read and agreed to the published version of the manuscript.

**Funding:** The study is funded by Deutsche Forschungsgemeinschaft (DFG), the German Research Foundation (BU3075/2-1 and KI2434/1-2). The funding foundation was not involved in trial design, patient recruitment, data collection, analysis, interpretation or presentation, writing or editing of the reports, or the decision to submit for publication. The corresponding author had full access to all data in the study and had all responsibility for the decision to submit for publication.

**Institutional Review Board Statement:** All procedures performed were in accordance with the ethical standards of the institutional research committee of the University Duisburg-Essen (study number 17-7396-BO) and Düsseldorf (study number 6040R) and with the principles of the 1964 Declaration of Helsinki and its later amendments. Informed consent was obtained from all individual participants included in the study.

**Informed Consent Statement:** Informed consent was obtained from all subjects involved in the study.

**Data Availability Statement:** The datasets used and/or analyzed during the current study are available from the corresponding author upon reasonable request.

**Acknowledgments:** This publication contains parts of the MD thesis of Cleo Stieglitz and is therefore in partial fulfillment of the requirements for an MD thesis at the Medical Faculty of the Heinrich-Heine University, Düsseldorf.

**Conflicts of Interest:** The authors declare no conflict of interest.

## References

1. Sung, H.; Ferlay, J.; Siegel, R.L.; Laversanne, M.; Soerjomataram, I.; Jemal, A.; Bray, F. Global cancer statistics 2020: GLOBOCAN estimates of incidence and mortality worldwide for 36 cancers in 185 countries. *CA Cancer J. Clin.* **2021**, *71*, 209–249. [\[CrossRef\]](#) [\[PubMed\]](#)
2. Bray, F.; Ferlay, J.; Soerjomataram, I.; Siegel, R.L.; Torre, L.A.; Jemal, A. Global cancer statistics 2018: GLOBOCAN estimates of incidence and mortality worldwide for 36 cancers in 185 countries. *CA Cancer J. Clin.* **2018**, *68*, 394–424. [\[CrossRef\]](#)
3. Rose, J.; Puckett, Y. Breast Reconstruction Free Flaps. In *StatPearls*; StatPearls Publishing LLC.: Treasure Island, FL, USA, 2022.
4. Goldhirsch, A.; Glick, J.H.; Gelber, R.D.; Coates, A.S.; Thürlimann, B.; Senn, H.J. Meeting highlights: International expert consensus on the primary therapy of early breast cancer 2005. *Ann. Oncol.* **2005**, *16*, 1569–1583. [\[CrossRef\]](#) [\[PubMed\]](#)
5. Bonnefoi, H.; Litière, S.; Piccart, M.; MacGrogan, G.; Fumoleau, P.; Brain, E.; Petit, T.; Rouanet, P.; Jassem, J.; Moldovan, C.; et al. Pathological complete response after neoadjuvant chemotherapy is an independent predictive factor irrespective of simplified breast cancer intrinsic subtypes: A landmark and two-step approach analyses from the EORTC 10994/BIG 1-00 phase III trial. *Ann. Oncol.* **2014**, *25*, 1128–1136. [\[CrossRef\]](#) [\[PubMed\]](#)
6. Groheux, D.; Hindie, E. Breast cancer: Initial workup and staging with FDG PET/CT. *Clin. Transl. Imaging* **2021**, *9*, 221–231. [\[CrossRef\]](#) [\[PubMed\]](#)
7. Shawky, M.; Ali, Z.A.E.; Hashem, D.H.; Houseni, M. Role of positron-emission tomography/computed tomography (PET/CT) in breast cancer. *Egypt. J. Radiol. Nucl. Med.* **2020**, *51*, 125. [\[CrossRef\]](#)
8. Han, S.; Choi, J.Y. Prognostic value of (18)F-FDG PET and PET/CT for assessment of treatment response to neoadjuvant chemotherapy in breast cancer: A systematic review and meta-analysis. *Breast Cancer Res.* **2020**, *22*, 119. [\[CrossRef\]](#)
9. Piscopo, L.; Nappi, C.; Volpe, F.; Romeo, V.; Nicolai, E.; Gallicchio, R.; Giordano, A.; Storto, G.; Pace, L.; Cavaliere, C.; et al. Prognostic Value of Hybrid PET/MR Imaging in Patients with Differentiated Thyroid Cancer. *Cancers* **2022**, *14*, 2958. [\[CrossRef\]](#)
10. Klain, M.; Nappi, C.; Nicolai, E.; Romeo, V.; Piscopo, L.; Giordano, A.; Gaudieri, V.; Zampella, E.; Pace, L.; Carlo, C.; et al. Comparison of simultaneous (18)F-2-[18F] FDG PET/MR and PET/CT in the follow-up of patients with differentiated thyroid cancer. *Eur. J. Nucl. Med. Mol. Imaging* **2020**, *47*, 3066–3073. [\[CrossRef\]](#)
11. Bruckmann, N.M.; Morawitz, J.; Fendler, W.P.; Ruckhäberle, E.; Bittner, A.K.; Giesel, F.L.; Herrmann, K.; Antoch, G.; Umutlu, L.; Kirchner, J. A Role of PET/MR in Breast Cancer? *Semin. Nucl. Med.* **2022**, *52*, 611–618. [\[CrossRef\]](#)
12. Murthy, V.; Sonni, I.; Jariwala, N.; Juarez, R.; Reiter, R.E.; Raman, S.S.; Hope, T.A. The Role of PSMA PET/CT and PET/MRI in the Initial Staging of Prostate Cancer. *Eur. Urol. Focus* **2021**, *7*, 258–266. [\[CrossRef\]](#) [\[PubMed\]](#)
13. Heacock, L.; Weissbrodt, J.; Raad, R.; Campbell, N.; Friedman, K.P.; Ponzo, F.; Chandarana, H. PET/MRI for the evaluation of patients with lymphoma: Initial observations. *AJR. Am. J. Roentgenol.* **2015**, *204*, 842–848. [\[CrossRef\]](#) [\[PubMed\]](#)
14. Kirchner, J.; Grueneisen, J.; Martin, O.; Oehmigen, M.; Quick, H.H.; Bittner, A.-K.; Hoffmann, O.; Ingenwerth, M.; Catalano, O.A.; Heusch, P.; et al. Local and whole-body staging in patients with primary breast cancer: A comparison of one-step to two-step staging utilizing 18F-FDG-PET/MRI. *Eur. J. Nucl. Med. Mol. Imaging* **2018**, *45*, 2328–2337. [\[CrossRef\]](#) [\[PubMed\]](#)
15. Bruckmann, N.M.; Kirchner, J.; Morawitz, J.; Umutlu, L.; Herrmann, K.; Bittner, A.K.; Hoffmann, O.; Mohrmann, S.; Ingenwerth, M.; Schaarschmidt, B.M.; et al. Prospective comparison of CT and 18F-FDG PET/MRI in N and M staging of primary breast cancer patients: Initial results. *PLoS ONE* **2021**, *16*, e0260804. [\[CrossRef\]](#)
16. Bruckmann, N.M.; Kirchner, J.; Umutlu, L.; Fendler, W.P.; Seifert, R.; Herrmann, K.; Bittner, A.-K.; Hoffmann, O.; Mohrmann, S.; Antke, C.; et al. Prospective comparison of the diagnostic accuracy of 18F-FDG PET/MRI, MRI, CT, and bone scintigraphy for the detection of bone metastases in the initial staging of primary breast cancer patients. *Eur. Radiol.* **2021**, *31*, 8714–8724. [\[CrossRef\]](#)
17. Sawicki, L.M.; Grueneisen, J.; Schaarschmidt, B.M.; Buchbender, C.; Nagarajah, J.; Umutlu, L.; Antoch, G.; Kinner, S. Evaluation of 18F-FDG PET/MRI, 18F-FDG PET/CT, MRI, and CT in whole-body staging of recurrent breast cancer. *Eur. J. Radiol.* **2016**, *85*, 459–465. [\[CrossRef\]](#) [\[PubMed\]](#)



18. Grueneisen, J.; Nagarajah, J.; Buchbender, C.; Hoffmann, O.; Schaarschmidt, B.M.; Poeppel, T.; Forsting, M.; Quick, H.H.; Umutlu, L.; Kinner, S. Positron Emission Tomography/Magnetic Resonance Imaging for Local Tumor Staging in Patients With Primary Breast Cancer: A Comparison With Positron Emission Tomography/Computed Tomography and Magnetic Resonance Imaging. *Investig. Radiol.* **2015**, *50*, 505–513. [\[CrossRef\]](#)
19. Mann, R.M.; Cho, N.; Moy, L. Breast MRI: State of the Art. *Radiology* **2019**, *292*, 520–536. [\[CrossRef\]](#)
20. Morawitz, J.; Kirchner, J.; Martin, O.; Bruckmann, N.-M.; Dietzel, F.; Li, Y.; Rischpler, C.; Herrmann, K.; Umutlu, L.; Bittner, A.-K.; et al. Prospective Correlation of Prognostic Immunohistochemical Markers with SUV and ADC Derived from Dedicated Hybrid Breast 18F-FDG PET/MRI in Women with Newly Diagnosed Breast Cancer. *Clin. Nucl. Med.* **2020**, *Publish Ahead of Print*. [\[CrossRef\]](#)
21. Rosenkrantz, A.B.; Friedman, K.; Chandarana, H.; Melsaether, A.; Moy, L.; Ding, Y.S.; Jhaveri, K.; Beltran, L.; Jain, R. Current Status of Hybrid PET/MRI in Oncologic Imaging. *AJR Am. J. Roentgenol.* **2016**, *206*, 162–172. [\[CrossRef\]](#)
22. Hanahan, D.; Weinberg, R.A. Hallmarks of cancer: The next generation. *Cell* **2011**, *144*, 646–674. [\[CrossRef\]](#) [\[PubMed\]](#)
23. Harbeck, N.; Gnant, M. Breast cancer. *Lancet* **2017**, *389*, 1134–1150. [\[CrossRef\]](#) [\[PubMed\]](#)
24. Tan, T.J.; Chan, J.J.; Kamis, S.; Dent, R.A. What is the role of immunotherapy in breast cancer? *Chin. Clin. Oncol.* **2018**, *7*, 13. [\[CrossRef\]](#)
25. Leitlinienprogramm Onkologie (Deutsche Krebsgesellschaft, D.K.; AWMF). *S3-Leitlinie Früherkennung, Diagnose, Therapie und Nachsorge des Mammakarzinoms*; Version 4.4.; 2021, Berlin (AWMF, DKG, DKH). AWMF Registernummer: 032-045OL. Available online: <http://www.leitlinienprogramm-onkologie.de/leitlinien/mammakarzinom/> (accessed on 10 January 2023).
26. Hartkopf, A.D.; Wallwiener, M.; Hahn, M.; Fehm, T.N.; Brucker, S.Y.; Taran, F.A. Simultaneous Detection of Disseminated and Circulating Tumor Cells in Primary Breast Cancer Patients. *Cancer Res. Treat.* **2016**, *48*, 115–124. [\[CrossRef\]](#) [\[PubMed\]](#)
27. Friberg, S.; Nyström, A. Cancer Metastases: Early Dissemination and Late Recurrences. *Cancer Growth Metastasis* **2015**, *8*, 43–49. [\[CrossRef\]](#)
28. Pantel, K.; Brakenhoff, R.H.; Brandt, B. Detection, clinical relevance and specific biological properties of disseminating tumour cells. *Nat. Rev. Cancer* **2008**, *8*, 329–340. [\[CrossRef\]](#)
29. Hartkopf, A.D.; Brucker, S.Y.; Taran, F.A.; Harbeck, N.; von Au, A.; Naume, B.; Pierga, J.Y.; Hoffmann, O.; Beckmann, M.W.; Rydén, L.; et al. Disseminated tumour cells from the bone marrow of early breast cancer patients: Results from an international pooled analysis. *Eur. J. Cancer* **2021**, *154*, 128–137. [\[CrossRef\]](#)
30. Janvier, L.; Olivier, P.; Blonski, M.; Morel, O.; Vignaud, J.M.; Karcher, G.; Taillandier, L.; Verger, A. Correlation of SUV-Derived Indices With Tumoral Aggressiveness of Gliomas in Static 18F-FDOPA PET: Use in Clinical Practice. *Clin. Nucl. Med.* **2015**, *40*, e429–e435. [\[CrossRef\]](#)
31. Lee, D.W.; Chong, G.O.; Lee, Y.H.; Hong, D.G.; Cho, Y.L.; Jeong, S.Y.; Park, J.Y.; Lee, Y.S. Role of SUVmax and GLUT-1 Expression in Determining Tumor Aggressiveness in Patients With Clinical Stage I Endometrioid Endometrial Cancer. *Int. J. Gynecol. Cancer* **2015**, *25*, 843–849. [\[CrossRef\]](#)
32. Cerfolio, R.J.; Bryant, A.S.; Ohja, B.; Bartolucci, A.A. The maximum standardized uptake values on positron emission tomography of a non-small cell lung cancer predict stage, recurrence, and survival. *J. Thorac. Cardiovasc. Surg.* **2005**, *130*, 151–159. [\[CrossRef\]](#)
33. Song, P.J.; Lu, Q.Y.; Li, M.Y.; Li, X.; Shen, F. Comparison of effects of 18F-FDG PET-CT and MRI in identifying and grading gliomas. *J. Biol. Regul. Homeost. Agents* **2016**, *30*, 833–838.
34. Incoronato, M.; Grimaldi, A.M.; Cavaliere, C.; Inglese, M.; Mirabelli, P.; Monti, S.; Ferbo, U.; Nicolai, E.; Soricelli, A.; Catalano, O.A.; et al. Relationship between functional imaging and immunohistochemical markers and prediction of breast cancer subtype: A PET/MRI study. *Eur. J. Nucl. Med. Mol. Imaging* **2018**, *45*, 1680–1693. [\[CrossRef\]](#)
35. Catalano, O.A.; Horn, G.L.; Signore, A.; Iannace, C.; Lepore, M.; Vangel, M.; Luongo, A.; Catalano, M.; Lehman, C.; Salvatore, M.; et al. PET/MR in invasive ductal breast cancer: Correlation between imaging markers and histological phenotype. *Br. J. Cancer* **2017**, *116*, 893–902. [\[CrossRef\]](#) [\[PubMed\]](#)
36. Surov, A.; Meyer, H.J.; Wienke, A. Associations Between PET Parameters and Expression of Ki-67 in Breast Cancer. *Transl. Oncol.* **2019**, *12*, 375–380. [\[CrossRef\]](#) [\[PubMed\]](#)
37. Buchbender, C.; Heusner, T.A.; Lauenstein, T.C.; Bockisch, A.; Antoch, G. Oncologic PET/MRI, part 2: Bone tumors, soft-tissue tumors, melanoma, and lymphoma. *J. Nucl. Med.* **2012**, *53*, 1244–1252. [\[CrossRef\]](#) [\[PubMed\]](#)
38. Razek, A.A. Diffusion magnetic resonance imaging of chest tumors. *Cancer Imaging* **2012**, *12*, 452–463. [\[CrossRef\]](#)
39. Guo, Y.; Cai, Y.Q.; Cai, Z.L.; Gao, Y.G.; An, N.Y.; Ma, L.; Mahankali, S.; Gao, J.H. Differentiation of clinically benign and malignant breast lesions using diffusion-weighted imaging. *J. Magn. Reson. Imaging* **2002**, *16*, 172–178. [\[CrossRef\]](#) [\[PubMed\]](#)
40. Sinha, S.; Lucas-Quesada, F.A.; Sinha, U.; DeBruhl, N.; Bassett, L.W. In vivo diffusion-weighted MRI of the breast: Potential for lesion characterization. *J. Magn. Reson. Imaging* **2002**, *15*, 693–704. [\[CrossRef\]](#) [\[PubMed\]](#)
41. Association, W.M. World Medical Association Declaration of Helsinki: Ethical Principles for Medical Research Involving Human Subjects. *JAMA* **2013**, *310*, 2191–2194. [\[CrossRef\]](#)
42. Oehmigen, M.; Lindemann, M.E.; Lanz, T.; Kinner, S.; Quick, H.H. Integrated PET/MR breast cancer imaging: Attenuation correction and implementation of a 16-channel RF coil. *Med. Phys.* **2016**, *43*, 4808. [\[CrossRef\]](#)
43. Quick, H. Integrated PET/MR. *J. Magn. Reson. Imaging* **2014**, *39*, 243–258. [\[CrossRef\]](#) [\[PubMed\]](#)

44. Paulus, D.H.; Quick, H.H.; Geppert, C.; Fenchel, M.; Zhan, Y.; Hermosillo, G.; Faul, D.; Boada, F.; Friedman, K.P.; Koesters, T. Whole-Body PET/MR Imaging: Quantitative Evaluation of a Novel Model-Based MR Attenuation Correction Method Including Bone. *J. Nucl. Med.* **2015**, *56*, 1061–1066. [CrossRef] [PubMed]
45. Kartmann, R.; Paulus, D.H.; Braun, H.; Aklan, B.; Ziegler, S.; Navalpakkam, B.K.; Lentschig, M.; Quick, H.H. Integrated PET/MR imaging: Automatic attenuation correction of flexible RF coils. *Med. Phys.* **2013**, *40*, 82301. [CrossRef]
46. AGO e. V. Guidelines Breast. Available online: [https://www.ago-online.de/fileadmin/ago-online/downloads/\\_leitlinien/kommission\\_mamma/2022/englisch/Einzeldateien/AGO\\_2022E\\_02\\_Breast\\_Cancer\\_Risk\\_Genetics\\_and\\_Prevention.pdf](https://www.ago-online.de/fileadmin/ago-online/downloads/_leitlinien/kommission_mamma/2022/englisch/Einzeldateien/AGO_2022E_02_Breast_Cancer_Risk_Genetics_and_Prevention.pdf) (accessed on 5 December 2022).
47. Prat, A.; Pineda, E.; Adamo, B.; Galván, P.; Fernández, A.; Gaba, L.; Díez, M.; Viladot, M.; Arance, A.; Muñoz, M. Clinical implications of the intrinsic molecular subtypes of breast cancer. *Breast* **2015**, *24*, S26–S35. [CrossRef] [PubMed]
48. van't Veer, L.J.; Paik, S.; Hayes, D.F. Gene expression profiling of breast cancer: A new tumor marker. *J. Clin. Oncol.* **2005**, *23*, 1631–1635. [CrossRef]
49. Fehm, T.; Braun, S.; Muller, V.; Janni, W.; Gebauer, G.; Marth, C.; Schindlbeck, C.; Wallwiener, D.; Borgen, E.; Naume, B.; et al. A concept for the standardized detection of disseminated tumor cells in bone marrow from patients with primary breast cancer and its clinical implementation. *Cancer* **2006**, *107*, 885–892. [CrossRef]
50. Kasimir-Bauer, S.; Reiter, K.; Aktas, B.; Bittner, A.K.; Weber, S.; Keller, T.; Kimmig, R.; Hoffmann, O. Different prognostic value of circulating and disseminated tumor cells in primary breast cancer: Influence of bisphosphonate intake? *Sci. Rep.* **2016**, *6*, 26355. [CrossRef]
51. Borgen, E.; Naume, B.; Nesland, J.M.; Kvalheim, G.; Beiske, K.; Fodstad, O.; Diel, I.; Solomayer, E.F.; Theocharous, P.; Coombes, R.C.; et al. Standardization of the immunocytochemical detection of cancer cells in BM and blood: I. establishment of objective criteria for the evaluation of immunostained cells. *Cytotherapy* **1999**, *1*, 377–388. [CrossRef]
52. Li, J.; Zhao, M.; Yuan, L.; Liu, Y.; Ma, N. [Correlation and Influencing Factors of SUVmax and Ki-67 in Non-Hodgkin Lymphoma]. *Zhongguo Shi Yan Xue Ye Xue Za Zhi* **2022**, *30*, 136–140. [CrossRef]
53. Shen, G.-h.; Hu, S.; Liu, B.; Kuang, A.r. Degree of SUVmax correlates with Ki-67 index in patients with breast cancer: A meta-analysis. *Int. J. Clin. Exp. Pathol.* **2017**, *10*, 1488–1498.
54. Kitajima, K.; Yamano, T.; Fukushima, K.; Miyoshi, Y.; Hirota, S.; Kawanaka, Y.; Miya, M.; Doi, H.; Yamakado, K.; Hirota, S. Correlation of the SUVmax of FDG-PET and ADC values of diffusion-weighted MR imaging with pathologic prognostic factors in breast carcinoma. *Eur. J. Radiol.* **2016**, *85*, 943–949. [CrossRef]
55. Nakamura, K.; Kodama, J.; Okumura, Y.; Hongo, A.; Kanazawa, S.; Hiramatsu, Y. The SUVmax of <sup>18</sup>F-FDG PET Correlates With Histological Grade in Endometrial Cancer. *Int. J. Gynecol. Cancer* **2010**, *20*, 110–115. [CrossRef] [PubMed]
56. Sanli, Y.; Kuyumcu, S.; Ozkan, Z.G.; Işık, G.; Karanlık, H.; Guzelbey, B.; Turkmen, C.; Ozel, S.; Yavuz, E.; Mudun, A. Increased FDG uptake in breast cancer is associated with prognostic factors. *Ann. Nucl. Med.* **2012**, *26*, 345–350. [CrossRef] [PubMed]
57. Yerushalmi, R.; Woods, R.; Ravdin, P.M.; Hayes, M.M.; Gelmon, K.A. Ki67 in breast cancer: Prognostic and predictive potential. *Lancet Oncol.* **2010**, *11*, 174–183. [CrossRef]
58. Haroon, S.; Hashmi, A.A.; Khurshid, A.; Kanpurwala, M.A.; Mujtuba, S.; Malik, B.; Faridi, N. Ki67 index in breast cancer: Correlation with other prognostic markers and potential in pakistani patients. *Asian Pac. J. Cancer Prev.* **2013**, *14*, 4353–4358. [CrossRef]
59. Afkari, H.; Makrufardi, F.; Hidayat, B.; Budiawan, H.; Sundawa Kartamihardja, A.H. Correlation between ER, PR, HER-2, and Ki-67 with the risk of bone metastases detected by bone scintigraphy in breast cancer patients: A cross sectional study. *Ann. Med. Surg.* **2021**, *67*, 102532. [CrossRef]
60. Koo, H.R.; Park, J.S.; Kang, K.W.; Cho, N.; Chang, J.M.; Bae, M.S.; Kim, W.H.; Lee, S.H.; Kim, M.Y.; Kim, J.Y.; et al. 18F-FDG uptake in breast cancer correlates with immunohistochemically defined subtypes. *Eur. Radiol.* **2014**, *24*, 610–618. [CrossRef] [PubMed]
61. Hegazy, R.; Azzam, H. Value of apparent diffusion coefficient factor in correlation with the molecular subtypes, tumor grade, and expression of Ki-67 in breast cancer. *Egypt. J. Radiol. Nucl. Med.* **2022**, *53*, 198. [CrossRef]
62. Park, E.K.; Cho, K.R.; Seo, B.K.; Woo, O.H.; Cho, S.B.; Bae, J.W. Additional Value of Diffusion-Weighted Imaging to Evaluate Prognostic Factors of Breast Cancer: Correlation with the Apparent Diffusion Coefficient. *Iran J. Radiol.* **2016**, *13*, e33133. [CrossRef]
63. Sanaat, Z.; Nouri, O.; Khanzadeh, M.; Mostafaei, H.; Vahed, N.; Kabiri, N.; Khoei, R.A.A.; Salehi-Pourmehr, H. Bisphosphonates and Prevention of the Perimenopausal Breast Cancer Recurrence: A Systematic Review and Meta-Analysis. *J. Breast Cancer* **2022**, *25*, 454–472. [CrossRef]
64. D'Oronzo, S.; Wood, S.; Brown, J.E. The use of bisphosphonates to treat skeletal complications in solid tumours. *Bone* **2021**, *147*, 115907. [CrossRef] [PubMed]
65. Diel, I.J.; Jaschke, A.; Solomayer, E.F.; Gollan, C.; Bastert, G.; Sohn, C.; Schuetz, F. Adjuvant oral clodronate improves the overall survival of primary breast cancer patients with micrometastases to the bone marrow: A long-term follow-up. *Ann. Oncol.* **2008**, *19*, 2007–2011. [CrossRef] [PubMed]
66. Diel, I.J.; Solomayer, E.F.; Costa, S.D.; Gollan, C.; Goerner, R.; Wallwiener, D.; Kaufmann, M.; Bastert, G. Reduction in new metastases in breast cancer with adjuvant clodronate treatment. *N. Engl. J. Med.* **1998**, *339*, 357–363. [CrossRef]

67. Hoffmann, O.; Schroer-Zuendorf, I.A.; Kasimir-Bauer, S.; Oberhoff, C.; Kimmig, R.; Heubner, M. Evaluation of the prognostic significance of disseminated tumor cells in the bone marrow of primary, non-metastatic breast cancer patients after a 7-year follow-up. *Arch. Gynecol. Obs.* **2015**, *292*, 1117–1125. [[CrossRef](#)] [[PubMed](#)]
68. Hoffmann, O.; Aktas, B.; Goldnau, C.; Heubner, M.; Oberhoff, C.; Kimmig, R.; Kasimir-Bauer, S. Effect of ibandronate on disseminated tumor cells in the bone marrow of patients with primary breast cancer: A pilot study. *Anticancer Res.* **2011**, *31*, 3623–3628. [[PubMed](#)]
69. Hartkopf, A.D.; Banys, M.; Krawczyk, N.; Wallwiener, M.; Schneck, H.; Neubauer, H.; Fehm, T. Circulating Tumor Cells in Early-Stage Breast Cancer. *Geburtshilfe Frauenheilkd* **2011**, *71*, 1067–1072. [[CrossRef](#)]
70. Schindlbeck, C.; Andergassen, U.; Hofmann, S.; Jückstock, J.; Jeschke, U.; Sommer, H.; Friese, K.; Janni, W.; Rack, B. Comparison of circulating tumor cells (CTC) in peripheral blood and disseminated tumor cells in the bone marrow (DTC-BM) of breast cancer patients. *J. Cancer Res. Clin. Oncol.* **2013**, *139*, 1055–1062. [[CrossRef](#)]
71. Balic, M.; Lin, H.; Young, L.; Hawes, D.; Giuliano, A.; McNamara, G.; Datar, R.H.; Cote, R.J. Most early disseminated cancer cells detected in bone marrow of breast cancer patients have a putative breast cancer stem cell phenotype. *Clin. Cancer Res.* **2006**, *12*, 5615–5621. [[CrossRef](#)]
72. Reuben, J.M.; Lee, B.N.; Gao, H.; Cohen, E.N.; Mego, M.; Giordano, A.; Wang, X.; Lodhi, A.; Krishnamurthy, S.; Hortobagyi, G.N.; et al. Primary breast cancer patients with high risk clinicopathologic features have high percentages of bone marrow epithelial cells with ALDH activity and CD44<sup>+</sup>CD24<sup>lo</sup> cancer stem cell phenotype. *Eur. J. Cancer* **2011**, *47*, 1527–1536. [[CrossRef](#)]
73. Kallergi, G.; Hoffmann, O.; Bittner, A.-K.; Papadimitriou, L.; Katsarou, S.D.; Zacharopoulou, N.; Zervakis, M.; Sfakianakis, S.; Stournaras, C.; Georgoulas, V.; et al. CXCR4 and JUNB double-positive disseminated tumor cells are detected frequently in breast cancer patients at primary diagnosis. *Ther. Adv. Med. Oncol.* **2020**, *12*, 1758835919895754. [[CrossRef](#)]
74. Kolb, A.D.; Shupp, A.B.; Mukhopadhyay, D.; Marini, F.C.; Bussard, K.M. Osteoblasts are “educated” by crosstalk with metastatic breast cancer cells in the bone tumor microenvironment. *Breast Cancer Res.* **2019**, *21*, 31. [[CrossRef](#)] [[PubMed](#)]

**Disclaimer/Publisher’s Note:** The statements, opinions and data contained in all publications are solely those of the individual author(s) and contributor(s) and not of MDPI and/or the editor(s). MDPI and/or the editor(s) disclaim responsibility for any injury to people or property resulting from any ideas, methods, instructions or products referred to in the content.